Journal of Marine Science and Application (2021) 20:546–557
https://doi.org/10.1007/s11804-021-00220-3

RESEARCH ARTICLE

Sinusoidal Vertical Motion Suppression and Flow Noise Calculation for a Sonobuoy

Chunlong Huang [1,2] · Kunde Yang [1,2] · Qiulong Yang [1,2] · Hui Li [1,2] · Yuanliang Ma [1,2]

Received: 12 June 2020 / Accepted: 13 June 2021 / Published online: 10 August 2021

Abstract
The flow noise associated with sinusoidal vertical motion of a sonobuoy restrains its working performance. In practice, a suspension system consisting of elastic suspension cable and isolation mass is adopted to isolate the hydrophone from large vertical motions of the buoy on the ocean surface. In the present study, a theoretical model of vertical motion based on the sonobuoy suspension system was proposed. The vertical motion velocity response of the hydrophone of a sonobuoy can be obtained by solving the theoretical model with Runge-Kutta algorithm. The flow noise of the hydrophone at this response motion velocity was predicted using a hybrid computational fluid dynamics (CFD)-Ffowcs Williams-Hawkings (FW-H) technique. The simulation results revealed that adding the elastic suspension cable with an appropriate elastic constant and counterweight with an appropriate mass have a good effect on reducing the flow noise caused by the sonobuoy vertical motion. The validation of this hybrid computational method used for reliable prediction of flow noise was also carried out on the basis of experimental data and empirical formula. The finds of this study can supply the deep understandings of the relationships between flow noise reduction and sonobuoy optimization.

Keywords Sonobuoy · Vertical motion · Flow noise · Differential equation of motion · Suspension system · Hydrophone

1 Introduction

As one of the main underwater acoustic detection tools, the sonobuoy has great importance in underwater object localization and ambient noise record (Barlow et al. 2018; Tan et al. 2011; Tollefsen and Sagen 2013, 2014). However, the flow noise caused by vertical motion2.2 of the sonobuoy limits its working performance. Since the surface buoy of the sonobuoy will move up and down with the sea waves, and this forced movement can be transmitted to underwater hydrophones by the cable, which causes relative movement between the hydrophone and the surrounding seawater. As a result, it generates pressure fluctuations on the hydrophone surface, which can be sensed by the hydrophone (Auvinen et al. 2019). In some cases, the noise level of the flow noise is much greater than the noise level of ambient noise, which reduces the signal-to-noise ratio (SNR) of the sonobuoy (Holler 2014; Willis et al. 2013). Moreover, according to the research of McEachern (1995), the flow noise can be generated even at very small stream velocity. As the detected target grows quieter, reducing the flow noise of sonobuoy is of great significance for improving working the performance of the sonobuoy.

The flow noise of the sonobuoy studied in this paper is generated from the pressure fluctuations which are caused by the sinusoidal vertical motion of the hydrophone. Therefore, it should to decouple the underwater hydrophone of the sonobuoy from the large vertical motions of the buoy on the sea surface. Kebe (1981) studied the self-noise of a suspended hydrophone on a moored sonobuoy. Some design

Article Highlights
- A suspension system consisting of an elastic suspension cable and isolation mass was studied in details.
- A theoretical model of vertical motion based on the sonobuoy suspension system was given.
- A numerical calculation method based on CFD and FW-H was adopted to compute the flow noise of the sonobuoy combining the theoretical model.

✉ Qiulong Yang
yangqiulong@nwpu.edu.cn

[1] School of Marine Science and Technology, Northwestern Polytechnical University, Xi'an 710072, China

[2] Key Laboratory of Ocean Acoustics and Sensing (Northwestern Polytechnical University), Ministry of Industry and Information Technology, Xi'an 710072, People's Republic of China

criteria were given, and an equation for calculating the optimal length of the expandable rubber band was discussed in particular. Additionally, Gobat and Grosenbaugh (1997) detailed efforts to reduce the flow noise received by hydrophones on a surface suspended sonobuoy by combining the analysis of experimental data. The relationships between flow noise and acceleration of the hydrophone were discussed. The structure of the sonobuoy was improved, including replacing the array and the surface buoy with a single flow-shield hydrophone and a spar buoy, respectively. Chapman (2008) studied the sinusoidal vertical motion of the sonobuoy suspension by experiment. A low-pass mechanical filter comprising a bungee cord and a damper disk was employed to isolate the acoustic sensor from the large vertical motion of the buoy on the ocean surface. Huang et al. (2018) studied the flow noise of hydrophone caused by vertical heave of sonobuoy with mathematical and simulation calculations. They found that choosing bungee cords with appropriate elastic coefficients can effectively suppress the heave thus reduce the flow noise of sonobuoy. Additionally, Guan et al. (2020) also studied the sonobuoy suspension system composed of bungee cord and damping disk and established a mathematical model considering its added mass and non-constant drag coefficient.

Besides, the suppression effects of the suspension system on flow noise also need to be verified. The flow noise can be obtained by experiment and numerical calculation. Numerical calculation has the advantage of avoiding interference from other noise signals compared with experimental measurement. However, in those researches mentioned above, the flow noise of the sonobuoy was almost obtained by experiment. Numerical studies of the flow noise were started with Lighthill's acoustic analogy theory (Lighthill 1952, 1954). In recent year, the Ffowcs Williams-Hawkings (FW-H) equation (Ffowcs Williams and Hawkings 1969 which was developed from Lighthill equation has been used for the prediction of the underwater flow noise; e.g., Kellett et al. (2013), Ozden et al. (2016), Huang et al. (2019) and Khalid et al. (2019) used the CFD-based unsteady fluid field calculation approach, coupled with the FW-H equation for noise prediction. In this study, a hybrid numerical method was adopted to calculate the flow noise of the sonobuoy under time-varying stream velocity.

In this paper, a suspension system consisting of an elastic suspension cable and isolation mass was studied in details. The suspension system allows the surface buoy to follow the large vertical motions of the sea surface while leaving the sensitive hydrophone at the lower end relatively undisturbed, thereby reducing the flow noise caused by the vertical motion of hydrophone. In order to analyze the vertical motion of the optimized sonobuoy under different conditions, a theoretical motion model of the sonobuoy was given. The suppression laws of the suspension cable elastic constant, underwater part mass of the sonobuoy and sea wave period on hydrophone vertical motions were given. Combining the theoretical model of motion, a numerical calculation method based on CFD and FW-H was adopted to compute the flow noise of the sonobuoy, which can be used to evaluate the effect of suspension system on reducing flow noise. The paper is arranged as follows: Section II gives a theoretical vibration model based on sonobuoy and obtains the velocity responses under different parameters. Section III introduces the mathematical model for calculating flow noise. Section IV presents the simulation results of the velocity responses and the flow noise under different conditions and Sec. V summarizes the conclusions.

2 Theoretical Model

2.1 Differential Equation of Vertical Motion

This study focuses on reducing the flow noise caused by the sinusoidal vertical motion of sonobuoy. As the relative movement between the hydrophone and the seawater is caused by the sea waves, therefore, an elastic suspension cable and isolation mass were added to the sonobuoy to decouple the vertical motion of the buoy at the sea surface from the underwater hydrophones. Figure 1 depicts the structure diagram of the sonobuoy with a suspension system. The elastic suspension cable 3 is added between the surface buoy 1 and the cable 4, and the underwater part below the suspension cable includes cable 4, hydrophone 5, and counterweight 6. Sonobuoy can be divided into two parts: the surface part and the underwater part. The elastic suspension cable plays a damper between the two parts. The underwater part can be seen as a forced vibration system when the sonobuoy drifts in the sea surface. After analyzing the forces acting on the underwater part, we found that there are three kinds of force, i.e., an external force

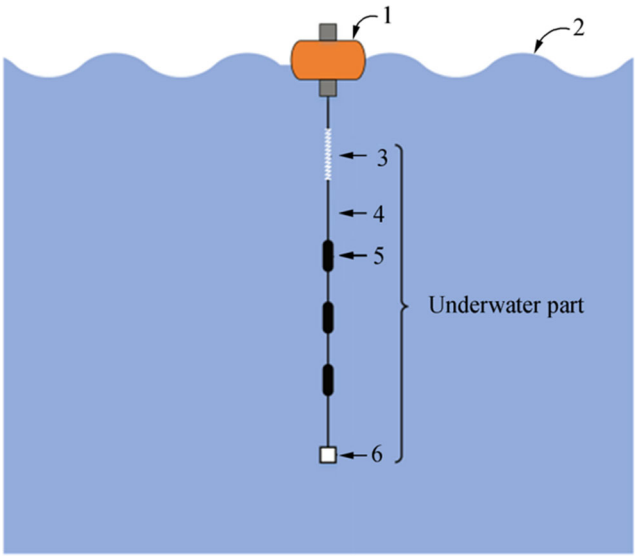

Fig. 1 Diagrammatic sketch of sonobuoy with a suspension system

from the surface buoy which caused by the sea wave, the total negative buoyancy, and drag force.

In order to analyze the vertical motion of the sonobuoy underwater part, a differential equation of motion of the underwater part was established, as shown in the following equation:

$$m\ddot{y} + ky = k(Y-L) - \Delta G - F \tag{1}$$

where

$$Y = d\sin(\omega t) \tag{2}$$

$$F = \frac{1}{2} CA\rho \dot{y}|\dot{y}| \tag{3}$$

m is the total mass of the underwater part of the sonobuoy. $\ddot{y}$ is the vertical motion acceleration, it equals d^2y / dt^2, and y is the displacement of the underwater part. k is the elastic constant of the elastic rope. Here, Y represents the external excitation; L is the total length of the cable and the elastic suspension cable in a natural stretch state, d is the wave height of the sea wave, ω is the angular frequency of the surface wave and it equals $2\pi / T$. T is the wave period. ΔG is the total negative buoyancy of the underwater part, and it equals to gravity minus its buoyancy. F is drag force. C is the drag coefficient, A is cross-sectional area of the sonobuoy, and ρ is the density of seawater. $\dot{y}$ is the vertical motion velocity, it equals dy/dt. In this study, the positive velocity represents that the sonobuoy is moving upward.

The differential equation of motion can be solved using the fourth order Runge-Kutta algorithm, shown as follows:

$$\begin{cases} y_{n+1} = y_n + \dfrac{h}{6}(K_1 + 2K_2 + 2K_3 + K_4), \\ K_1 = f(t_n, y_n), \\ K_2 = f\left(t_n + \dfrac{h}{2}, y_n + \dfrac{h}{2}K_1\right), \\ K_3 = f\left(t_n + \dfrac{h}{2}, y_n + \dfrac{h}{2}K_2\right), \\ K_4 = f(t_n + h, y_n + hK_3), \end{cases} \tag{4}$$

which has the accumulative error in order of $O(h^4)$, and h is calculation step. The implementation of the theoretical model is described in Algorithm 1

Algorithm 1 Calculation of the displacement and velocity responses for the hydrophone

Initialize y_{init} = - (L + ΔG / k) m, $\dot{y}_{init}$ = 0 m/s, t = [0:0.01:100] s and Δt = 0.01 s.
N = length(t).
for i = 1 : N
  Compute $Y(i)$ according to Eq. (2).
  if $\dot{y}(i)$ >= 0
    Compute $F(i)$ according to Eq. (3).
    else if $\dot{y}(i)$ < 0
    Compute $F(i)$ according to Eq. (3), then update $F(i)$ = - $F(i)$.
    end
  end
  if $Y(i) - y(i) > L$
    Update $t = t + 0.01$.
    Compute $y(i + 1)$ and $\dot{y}(i+1)$ according to Runge-Kutta method, i.e., Eq. (4).
    else if $Y(i) - y(i) <= L$
    Update $t = t + 0.01$.
    Update $\dot{y}(i+1) = \dot{y}(i) + ((F(i) - \Delta G) / m)\cdot\Delta t$ and $y(i + 1) = ((F(i) - \Delta G) / (2\cdot m)\cdot\Delta t + \dot{y}(i))\cdot\Delta t + y(i)$.
    end
  Update $y_{init} = y(i + 1)$ and $\dot{y}_{init} = \dot{y}(i+1)$.
  end
end

2.2 Velocity Response Simulation

In this subsection, the vertical motion velocity responses of the sonobuoy underwater part under different sea states were analyzed in details. Table 1 (Sea state table of wave and wind levels 2020) lists the average height and average period of sea surface waves under different sea states. As the sea state above level 5 is

Table 1 Wave parameters at different sea states

Sea state	Wave height h (m)	Wave period T (s)
Level 1	0.055	1.4
Level 2	0.183	2.4
Level 3	0.549	3.9
Level 4	1.311	5.4
Level 5	2.500	7.0

already quite bad, in this study, only sea states below level 5 are discussed.

It should be noted that the waveforms corresponding to different sea states are simplified into sine waves in this study. They are taken as the external excitations of the sonobuoy differential equation of motion. The fluid velocity is an important factor for flow noise. Therefore, in this section, a velocity transmission rate T_r is defined, which is used to evaluate the effect of the suspension system on suppressing the vertical motion caused by the waves, as shown below:

$$T_r = \frac{v_{max}}{V_{max}} \tag{5}$$

where v_{max} is the maximum response velocity of the hydrophone and V_{max} is the maximum motion velocity of the surface buoy caused by the sea wave. The smaller T_r means the oscillation amplitude of the hydrophone caused by the wave under the same sea state is smaller.

There is a maximum motion velocity V_{max} for the surface buoy at each sea state. Besides, we can obtain a series maximum response velocity v_{max} of the hydrophone under different elastic constant k with Algorithm 1 when the mass m of sonobuoy underwater part remains the same. Similarly, a series maximum response velocity v_{max} of the hydrophone under different mass m can be obtained by Algorithm 1 when the elastic constant k remains the same. Moreover, there is a maximum response velocity v_{max} of the hydrophone corresponding to different sea state when the elastic constant k and mass m keep unchanged. Then, we can obtain the relationships between T_r and k, m, and sea state by Eq. (5), respectively.

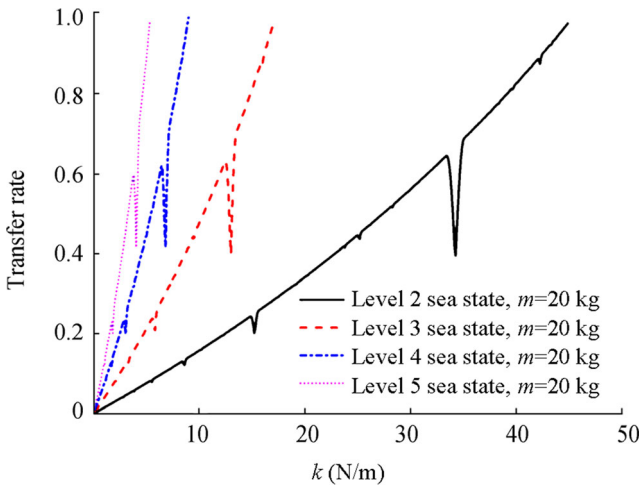

Fig. 2 Curve of T_r with k under different sea states

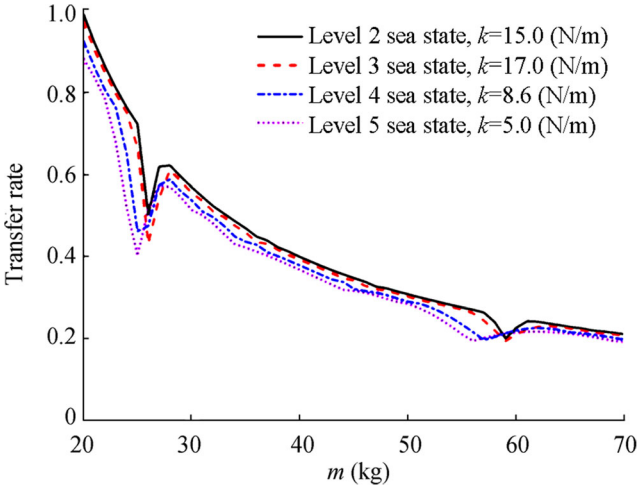

Fig. 3 Curve of T_r with m under different sea states

Figure 2 depicts the relationships between T_r and k under different sea states. It shows that in each sea state, the velocity transmission rate decreases with the decreasing elastic constant of the elastic suspension cable. Figure 3 depicts the relationships between T_r and m under different sea states. It is indicated that in each sea state, the velocity transmission rate decreases with increasing mass. Figure 4 shows the relationships between T_r and sea state. Here, $m = 20$ kg and $k = 5$ N/m. The results show that under the same condition, the velocity transmission rate gradually increases, while the sea state becomes worse. This is because the wave period increases when the sea state becomes worse.

Table 2 lists the value ranges of the elastic constant at different sea states when the transmission rate is less than or equals to 1 and the mass is 20 kg.

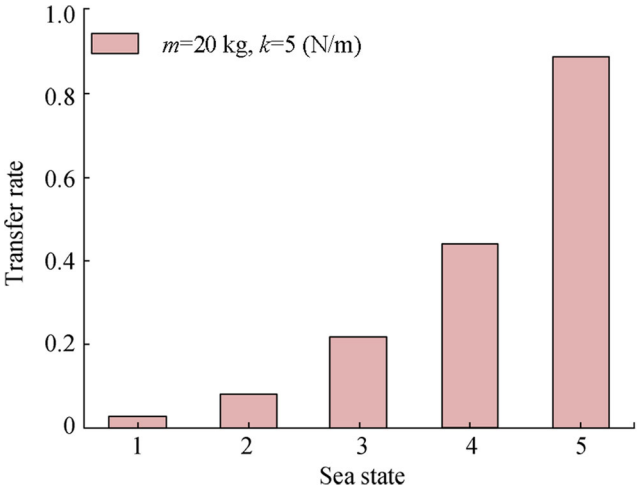

Fig. 4 Curve of T_r with sea state

Table 2 Elastic constant ranges at different sea states when $T_r \leq 1$ and m = 2 kg

Wave period T (s)	Elastic constant k (N/m)
1.4	≤ 134.570
2.4	≤ 45.820
3.9	≤ 17.352
5.4	≤ 9.050
7.0	≤ 5.385

Table 3 lists the value ranges of the mass at different sea states when the transmission rate is less than or equals to 1 and the elastic constant is 20 N/m.

By analyzing the data in Tables 2 and 3, it can be found that there is a relation between the wave angular frequency ω and the natural frequency ω_n. Among them, ω_n is the natural frequency of the sonobuoy, and $\omega_n = (k/m)^{0.5}$. When T_r is equal to 1, the specific value of ω_n and ω approximately is equal to 0.578. The relationship between ω_n and ω is shown in Fig. 5. The pink area below the curve of $\omega_n = 0.578\omega$ means that T_r is less than or equal to 1 under those conditions.

Consequently, through the analysis above, it can be concluded that T_r is related to the mass of the sonobuoy underwater part, the elastic constant of the elastic rope and the external excitation period, i.e., $T_r \propto (\omega_n/\omega)$.

3 Flow Noise Calculation Method

Flow noise predictions based on CFD and FW-H will be investigated in two steps, first solving the flow field, followed by the acoustic computations.

3.1 Flow Field Equations

According to the law of mass conservation and momentum conservation, the Navier-Stokes (NS) (Huang et al. 2019) equations of three-dimensional incompressible viscous fluids can be written as

$$\frac{\partial u_i}{\partial x_i} = 0 \tag{6}$$

Table 3 Mass ranges at different sea states when $T_r \leq 1$ and k = 20 N/m

Wave period T (s)	Mass m (kg)
1.4	≥ 2.968
2.4	≥ 8.722
3.9	≥ 23.033
5.4	≥ 44.157
7.0	≥ 74.201

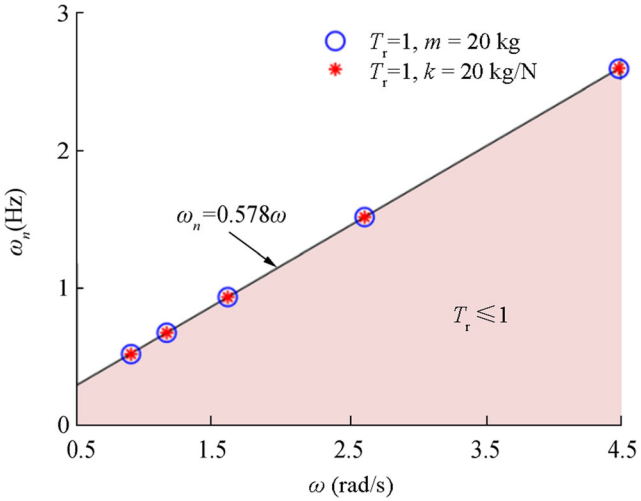

Fig. 5 The range of the ω_n in different sea states when T_r is less than or equal to 1

$$\frac{\partial u_i}{\partial t} + u_j \frac{\partial u_i}{\partial x_j} = f_i - \frac{1}{\rho}\frac{\partial p}{\partial x_i} + \frac{\partial}{\partial x_j}\left(\upsilon \frac{\partial u_i}{\partial x_j} - \overline{u_i' u_j'}\right) \tag{7}$$

where f_i is an external force and (x_i, x_j) denotes the particle coordinates and it is the function on t. u_i and u_j' are the average velocity and velocity fluctuation of the fluid, separately, i, j = 1,2,3, ρ is the density of the fluid, p is the average pressure, and υ is the kinematical viscosity coefficient. $\overline{u_i' u_j'}$ is the Reynolds stress.

In this study, the renormalization group (RNG) k-ε two-equation turbulence models were used to calculate the flow field (Yakhot et al. 1992; Li et al. 2011; Tahmasebi et al. 2020). The RNG model has an additional term in its ε equation that significantly improves the accuracy of rapidly strained flows. Moreover, the effect of swirl on turbulence is included in the RNG model, enhancing the accuracy for swirling flows. The RNG theory provides an analytical formula for turbulent Prandtl number but not a constant. This improvement achieves good results in the simulation accuracy and the range of application. Besides, it has a better performance for the calculation of complex shear flow in the transition region. The RNG k-ε two-equation turbulent model used in this paper is given by

$$\frac{\partial}{\partial t}(\rho k) + \frac{\partial}{\partial x_j}(\rho k u_j) = \frac{\partial}{\partial x_j}\left[\left(\mu + \frac{\mu_t}{\sigma_k}\right)\frac{\partial k}{\partial x_j}\right] + G_k - \rho\varepsilon \tag{8}$$

$$\frac{\partial}{\partial t}(\rho\varepsilon) + \frac{\partial}{\partial x_i}(\rho\varepsilon u_i) = \frac{\partial}{\partial x_j}\left[\left(\mu + \frac{\mu_t}{\sigma_\varepsilon}\right)\frac{\partial \varepsilon}{\partial x_j}\right] + C_{1\varepsilon}\frac{\varepsilon}{k}G_k - C_{2\varepsilon}\rho\frac{\varepsilon^2}{k} \tag{9}$$

$$G_k = \mu_t\left(\frac{\partial u_i}{\partial x_j} + \frac{\partial u_j}{\partial x_i}\right)\frac{\partial u_i}{\partial x_j} \tag{10}$$

where C_k is production rate of turbulent kinetic energy, and σ_k, σ_ε, $C_{1\varepsilon}$ and $C_{2\varepsilon}$ are constants of the model.

3.2 Acoustic Field Equations

The Lighthill acoustic analogy theory was derived from the Navier-Stokes equation, and the generalized Lighthill equation (Lighthill 1952, 1954) in acoustic analogy theory was used to calculate the noise field. Its wave density equation is in the form of

$$\frac{\partial^2 \rho'}{\partial t^2} - c_0^2 \nabla^2 \rho' = \frac{\partial^2 T_{ij}}{\partial x_i \partial x_j} \tag{11}$$

where ρ' is the density change by fluid disturbance, and $\rho' = \rho - \rho_0$, ρ denotes the fluid density with the disturbance and ρ_0 denotes the fluid density without the disturbance. c_0 is the sound speed in the isentropic fluid. T_{ij} is the Lighthill stress tensor, which is defined as (Kim and Yoon 2020)

$$T_{ij} = \rho u_i u_j + \left(p' - c_0^2 \rho'\right)\delta_{ij} - \tau_{ij} \tag{12}$$

where $p' = p - p_0$, and p and p_0 denote the pressure of the fluid with and without the disturbance, respectively; τ_{ij} denotes the viscous stress, and δ_{ij} is the Kronecker symbol.

In this paper, we use the FW-H equation (Ffowcs Williams and Hawkings 1969) which is developed from the Lighthill's equation to simulated the flow noise,

$$\begin{aligned} \frac{1}{c_0^2}\frac{\partial^2 p'}{\partial t^2} - \nabla^2 p' = {} & \frac{\partial^2}{\partial x_i \partial x_j}\left[T_{ij} H(f)\right] \\ & - \frac{\partial}{\partial x_i}\left\{\left[P_{ij} n_j + \rho u_i (u_n - v_n)\right]\delta(f)\right\} \\ & + \frac{\partial}{\partial t}\left\{\left[\rho_0 v_n + \rho(u_n - v_n)\right]\delta(f)\right\} \end{aligned} \tag{13}$$

in which vp' is the sound pressure of the far field, $\delta(f)$ is the Dirac delta function, and f is the wall function; $H(f)$ is Heaviside function; and n_j is the unit normal vector pointing from the periphery of the solid to the flow field. u_i and is the fluid velocity in the x_i direction; u_n and v_n denote the fluid velocity and surface velocity components normal to the surface. P_{ij} is the compressive stress tensor, which is defined as below:

$$P_{ij} = p\delta_{ij} - \mu\left[\frac{\partial u_i}{\partial x_j} + \frac{\partial u_j}{\partial x_i} - \frac{2}{3}\frac{\partial u_k}{\partial u_k}\delta_{ij}\right] \tag{14}$$

3.3 Validation of Simulated Flow Noise

The simulated flow noise of the hydrophone under a constant stream velocity was given, which has been verified by the experimental data. It should be noted that the experiment data were obtained from a submerged buoy rather than sonobuoy. Due to the lack of the flow noise experimental data of sonobuoy, the experimental data of flow noise received by the submerged buoy were selected to verify the simulated flow noise calculated by the hybrid numerical computation method in this study.

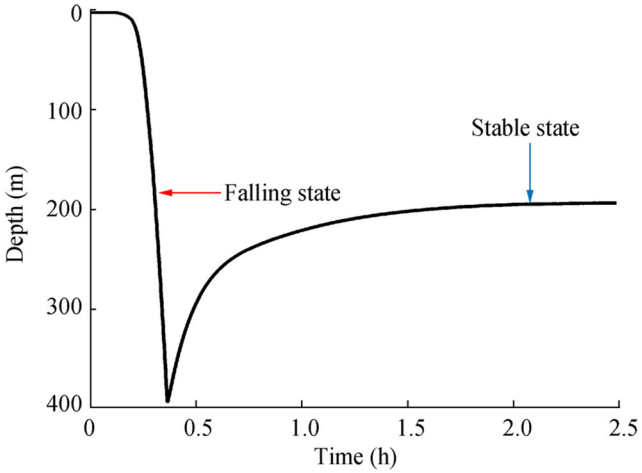

Fig. 6 Depth time series of hydrophone during descent process

The following figures show the noise data which was measured by a submerged buoy in a deep-water experiment in the South China Sea. There is flow noise generated on the hydrophone during the descent of the submerged buoy. The noise data were sampled continuously at 20 Hz. The descent velocity of the submerged buoy can be computed by the depth sensor. The depth change of a hydrophone on the submerged buoy is shown in Fig. 6. It shows that the submerged buoy will descend at an approximately constant speed before completely stabilizing on the bottom of the sea. The blue line in Fig. 7 depicts the noise level of the noise data recorded by a hydrophone when the submerged

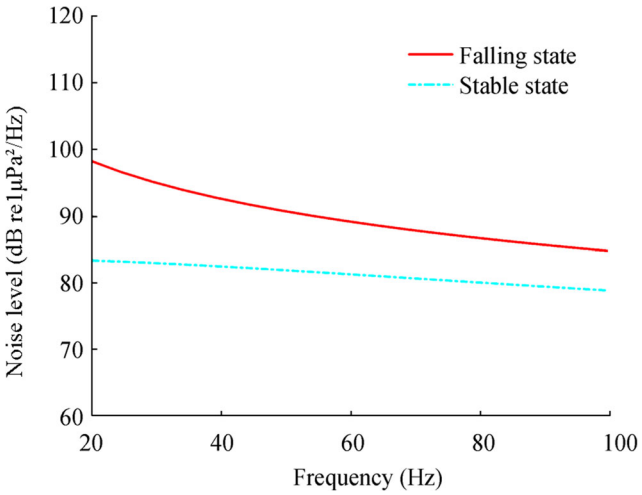

Fig. 7 The noise level of the data measured by experiments

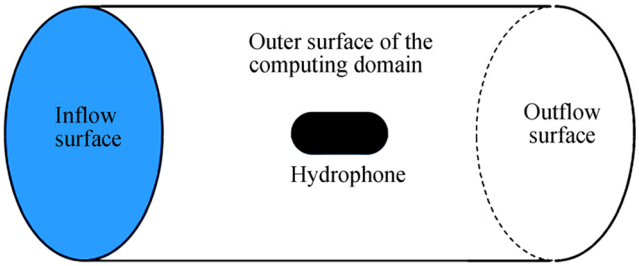

Fig. 8 The Computing Domain Used in CFD

buoy was stationary. The red line represents the noise level of the noise data received by the hydrophone when the submerged buoy was descending at a speed about of 1 m/s. In this study, the reference sound pressure for the noise level calculation is 10^{-6} Pa. The result shows that the noise level of the generated flow noise is higher than that of ambient noise. Thereby, it will reduce the SNR of the sonobuoy.

Next, we simulated the flow noise generated on the hydrophone of the submerged buoy during the descent with the numerical method. The relative movement between the hydrophone and the seawater can be seen as the seawater flowing past the stationary hydrophone at a certain stream velocity. The three-dimensional hydrophone model used for calculating the flow noise is shown in Fig. 8.

Flow noise calculation process:

(1) Establishing the model. The model was established regarding actual size of the hydrophone on the submerged buoy. The size ratio is 1:1. The maximum circumference and length of the hydrophone are 0.12 m and 0.10 m, respectively. The three-dimensional calculation domain used in CFD is a cylinder-topology, as shown in Fig. 8.
(2) Meshing the grid. In the calculation of CFD, the grid was chosen as body grid, which was created by commercial software ANSYS ICEM here. For the body grid, the non-dimensional spacing wall y^+ was set as 40, and the total number of the grid for the computational domain is about 0.85 million according to the y^+.
(3) Flow field calculation. The flow field was calculated with the FLUENT software. The flow field calculation boundary conditions are shown in Table 4. The RNG k-ε two-equation turbulent models were chosen in the flow field calculation. The finite volume method (FVW) was used to discrete the governing equations. The time step was set to be 10^{-3} s, the stream velocity of the inflow surface was set to be 1 m/s, and the liquid density is 1024 kg/m^3.
(4) Acoustic field calculation. The acoustic response of the flow field data was calculated with the FW-H integration approach. The sound speed is 1500 m/s.

Table 4 Boundary conditions of numerical calculation

Zone	Boundary conditions
Inflow surface	Velocity-inlet
Outflow surface	Outflow
Outer surface of the domain	Symmetry plane
Outer wall of the hydrophone	Non-slide wall

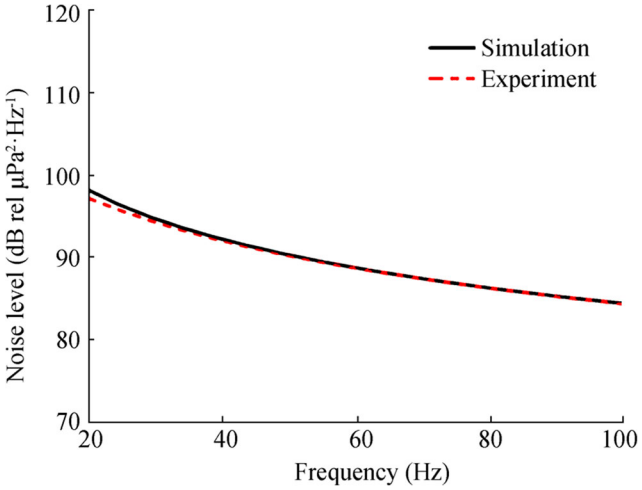

Fig. 9 The noise level of flow noise at a stream velocity of 1 m/s

The performance of the numerical calculation method is verified by the experiment data and empirical formula. Figure 9 shows the noise levels of flow noise obtained by numerical simulation and experiment at a stream velocity of 1 m/s. It depicts that the simulation result is in good agreement with that of the experimental data.

Besides, based on the Lighthill equation, Lauchle (1977) derived the relationship between the noise power G and free-

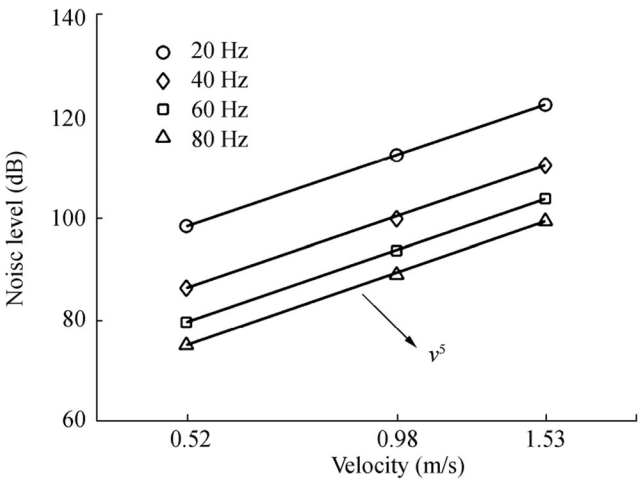

Fig. 10 Noise level of flow noise at different inflow velocities by simulation

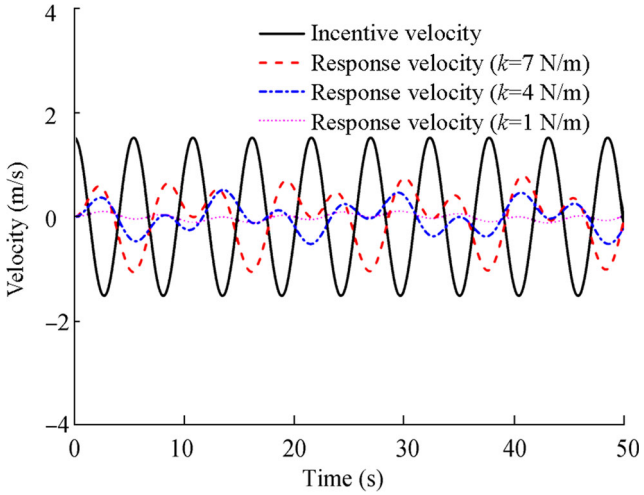

Fig. 11 The excitation velocity of a level 4 sea state and corresponding response velocity under different elastic constants (m = 20 kg)

stream velocity v by the method of dimensional analysis. The relationship is given by

$$G(f) \propto v^5 \tag{15}$$

In this paper, three sets flow noise under time varying incoming stream velocity were calculated, as shown in Figure 10. The maximum values of the three sets stream velocity are 0.52, 0.98, and 1.53 m/s, respectively. From Fig. 10, we can found that the noise levels at same frequency are proportional to the fifth power of stream velocities, which is consistent with the conclusion presented by Lauchle.

4 Flow Noise Numerical Simulation

A numerical method used for computing the flow noise of the sonobuoy is presented. The relative motion between the hydrophone and the seawater can be seen as the seawater flowing past the stationary hydrophone. The response velocities of the hydrophone under different conditions are obtained by solving the differential equation of motion. In this study, those response velocities are taken as the set value for the inflow surface by the User-Defined Function (UDF) to simulate the flow noise caused by the vertical motion of the hydrophone. The calculation process and boundary conditions are the same as those used in Sec. 3.3.

4.1 Different Elastic Coefficients

Figure 11 shows the incentive velocity under level 4 sea state and the response velocities of the hydrophone under different elastic constants. The incentive velocity is the vertical motion velocity of the surface buoy. When there is no elastic suspension cable on the sonobuoy, the response velocity of the hydrophone can be approximately replaced by the excitation velocity. The results show that the amplitude of these response velocities decreases with decreasing elastic constant.

Figure 12 shows the pressure fluctuations on the wall of hydrophones under different incoming stream velocities, which were calculated by CFD. Figure12 (a) shows the pressure fluctuation calculated by using the excitation velocity under the level 4 sea state as the inflow boundary condition.

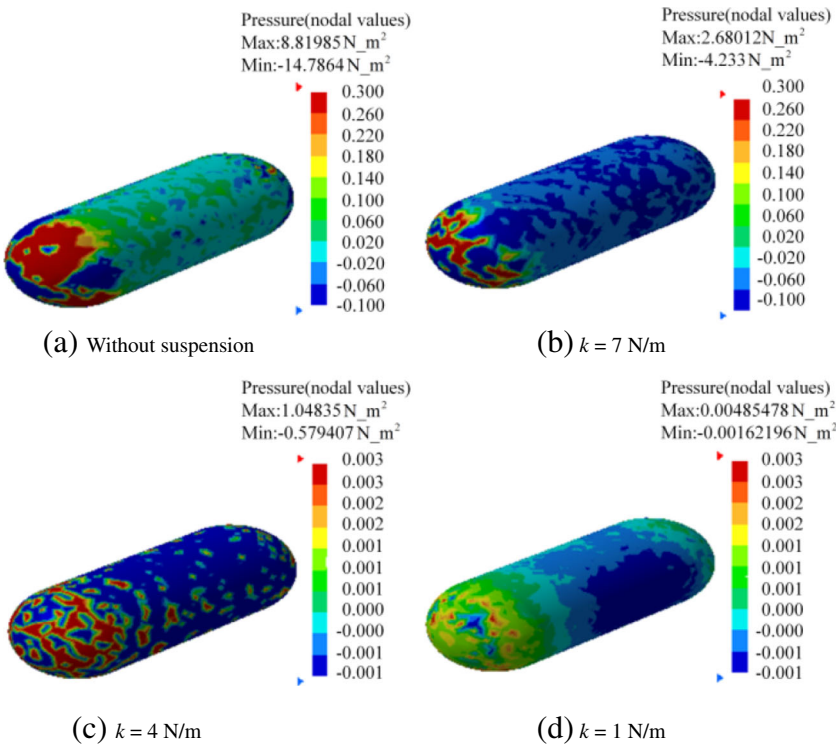

Fig. 12 The pressure fluctuation on the wall of hydrophone under different elastic constants (20 Hz)

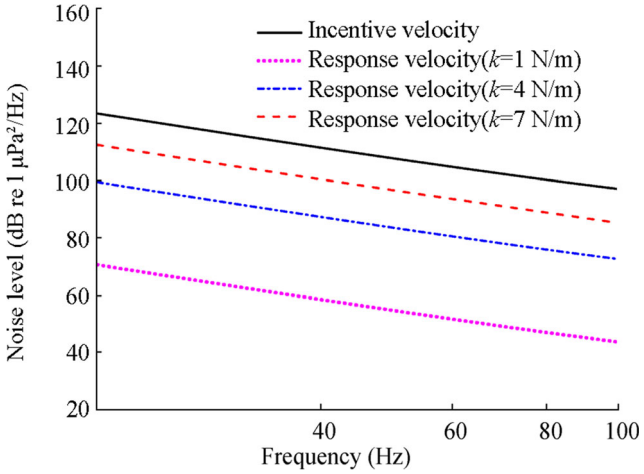

Fig. 13 The noise level of flow noise under different elastic constants

Figures 12(b)–12(d) show the wall pressure fluctuations on the hydrophone calculated by using the response velocities as the inflow boundary conditions, where the response velocities were obtained when the elastic constants equal 7, 4, and 1 N/m, respectively. Here, the sea state is level 4 and the mass m = 20 kg.

(a) Without suspension (b) k = 7 N/m

(c) k = 4 N/m (d) k = 1 N/m

It is indicated that the pressure fluctuations on the surface of the hydrophone gradually decrease with decreasing elastic constant of the elastic suspension cable. The pressure fluctuations shown in Fig. 12 were taken as the flow noise source and then computed their acoustic responses by the FW-H equation. The results are shown in Fig. 13. It is indicated that the noise level of the flow noise decreases with the decreasing elastic constant when the mass of the underwater part and the external excitation keep unchanged.

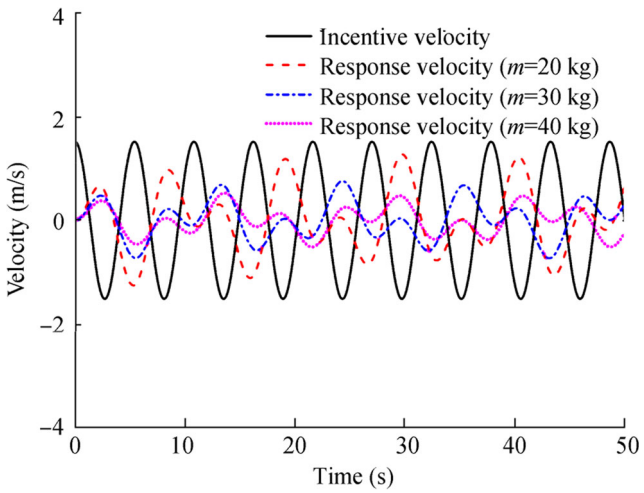

Fig. 14 The excitation velocity of level 4 sea state and corresponding response velocities under different masses (k = 8 N/m)

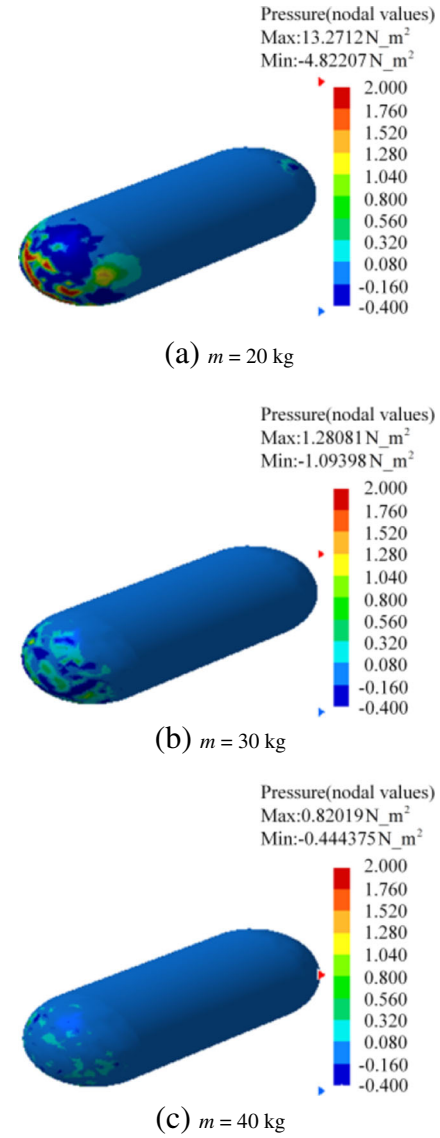

Fig. 15 The pressure fluctuation on the wall of hydrophone under different masses (20 Hz)

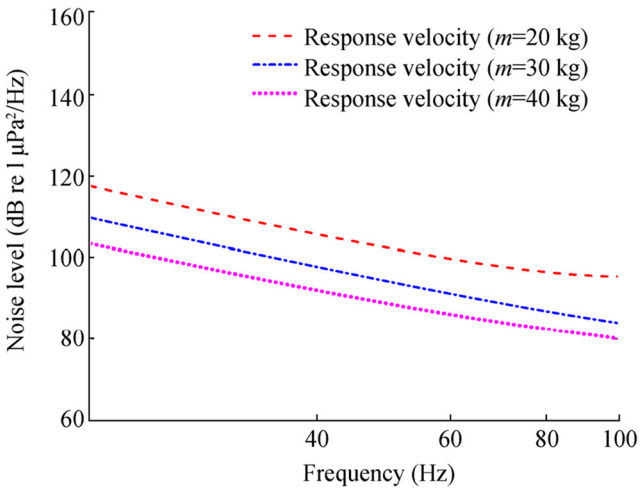

Fig. 16 The noise level of flow noise under different masses

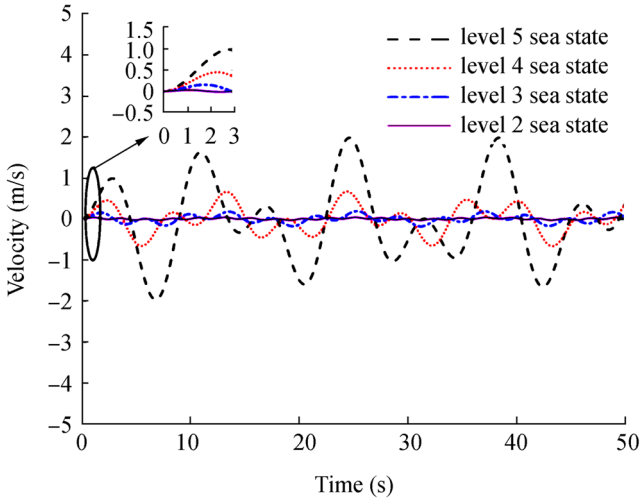

Fig. 17 Response velocity under different sea states (k = 5 N/m, m = 20 kg)

4.2 Different Masses

Figure 14 shows the incentive velocity under the level 4 sea state and the response velocities of the hydrophone under different masses. The results show that when the elastic constant and the external excitation keep unchanged, the amplitude of the response velocity becomes smaller with the increasing mass.

Figures 15(a)–(c) depict the wall pressure fluctuations on the hydrophones calculated by using the response velocities as the incoming stream boundary conditions, where the response velocities were obtained when the mass is 20, 30, and 40 kg, respectively. The response velocities in the aforementioned three cases were calculated when the sea state is 4 level and k is 8 N/m.

(a) m = 20 kg
(b) m = 30 kg
(c) m = 40 kg

Figure 15 shows that the wall pressure fluctuations on the surface on the hydrophones gradually decrease with increasing mass. The pressure fluctuations shown in Figure 15 were taken as the noise source and then calculate its acoustic responses using the FW-H equation. The curves in Figure 16 indicate that when the elastic constant and the external excitation keep unchanged, the noise level of the resulting flow noise decreases with increasing mass.

4.3 Different Sea States

Figure 17 shows the response velocities obtained under different sea states when k = 5 N/m and m = 20 kg. The results show that while the elastic constant and mass keep unchanged, the amplitude of response velocity is larger when the sea state becomes worse. This is because the wave period of the sea wave is gets larger as the sea state becomes worse.

Figures 18(a)–(d) depict the wall pressure fluctuations on the hydrophones, which were calculated by taking the response velocities obtained under different sea states as the

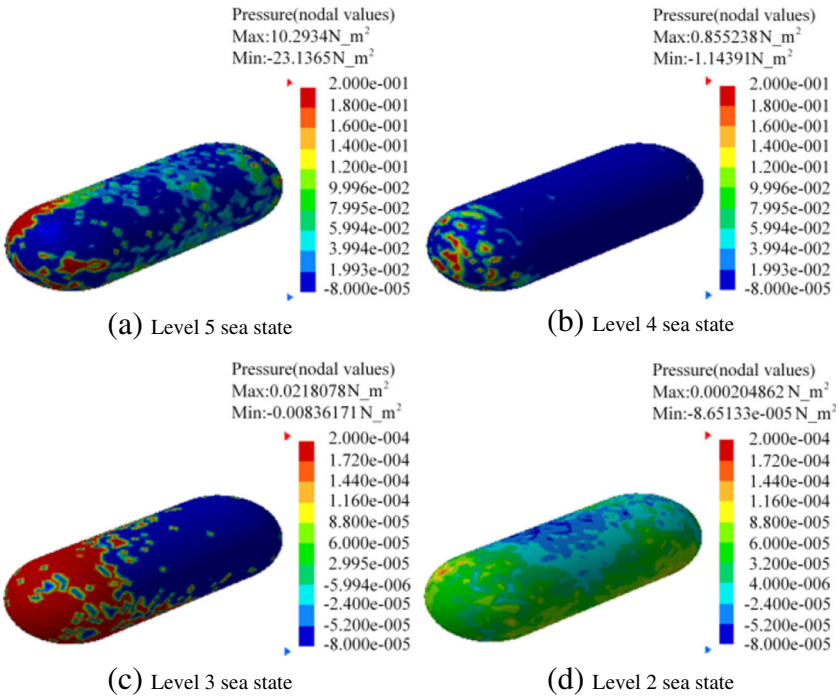

Fig. 18 The pressure fluctuation on the wall of hydrophone under different sea states (20 Hz)

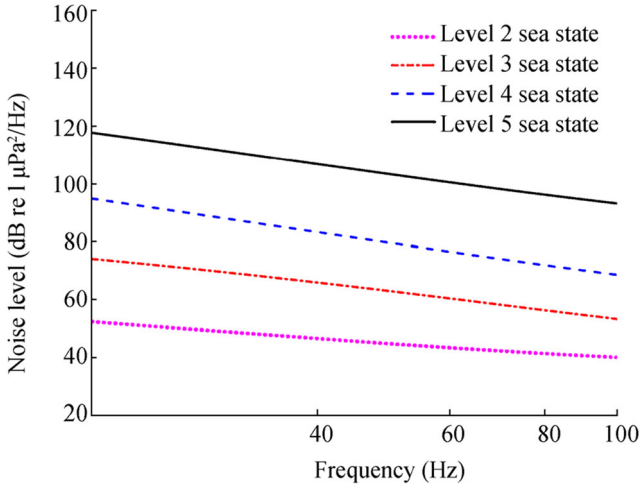

Fig. 19 The noise level of flow noise under different sea states

inflow boundary conditions. Here, it should be noted that $k = 5$ N/m and $m = 20$ kg.

(**a**) Level 5 sea state (**b**) Level 4 sea state

(**c**) Level 3 sea state (**d**) Level 2 sea state

Figure 18 shows that when the elastic constant and mass keep unchanged, the pressure fluctuations on the wall of the hydrophone will gradually increase as the sea state deteriorates. The pressure fluctuations in Fig. 18 were taken as the noise source in the calculation of the acoustic response with FW-H equation. The result is shown in Figure 19. It is indicated that the noise level of the flow noise becomes larger as the sea state becomes worse.

5 Conclusion and Discussion

In this study, a suspension system which consists of an elastic suspension cable and isolation mass was used to suppress the vertical motion of the sonobuoy. A theoretical model of motion based on the suspension system of the sonobuoy was given. The velocity responses of the optimized sonobuoy under different conditions were obtained by solving the dynamic differential equation. The suppression effects on hydrophone vertical motion of the elastic constant, the mass of the sonobuoy underwater part and the wave period were analyzed, respectively. Combining the theoretical model of motion, a hybrid numerical computation method based on CFD and FW-H was employed to compute the flow noise of the sonobuoy. The predicted flow noise can be used to evaluate the suppression effect of the suspension system on hydrophone vertical motion.

The main conclusions are obtained as follows:

(1) The suppression effect of the suspension system on the vertical motion of the hydrophone is mainly affected by elastic constant, mass, and wave period. Smaller elastic constant and larger mass can suppress the transmission of vertical motion better.

(2) Smaller transmission rate means better suppression effect, and the transfer rate is less than 1 while the ratio of ω_n and ω is smaller than 0.578.

(3) The hybrid numerical computation method for predicting the flow noise has good calculation accuracy. The simulation result was verified by the experiment data and empirical formula.

(4) The simulation results show that the suspension system has a good effect on reducing the flow noise of the sonobuoy caused by its vertical motion. At last, the experiment to confirm the vertical motion suppression effort and verify the flow noise of the sonobuoy computed by the numeral calculations will be the future work.

Funding This work was supported by the National Natural Science Foundation of China (Grant No. 61901383), the Natural Science Basic Research Plan in Shaanxi Province of China (Program No. 2019JQ633), the Fundamental Research Funds for the Central University (Grant No. 3102019HHZY030011), China Postdoctoral Science Foundation (2019M663822), and the Open Fund Project of Key Laboratory of Marine Environmental Information Technology, Ministry of Natural Resources of the People's Republic of China.

References

Auvinen MF, Barclay DR, Coffin MEW (2019) Performance of a Passive Acoustic Linear Array in a Tidal Channel. *IEEE J Ocean Eng* 45:1–10. https://doi.org/10.1109/JOE.2019.2944444

Barlow J, Griffiths ET, Klinck H, Harris DV (2018) Diving be havior of Cuvier's beaked whales inferred from three-dimensional acoustic localization and tracking using a nested array of drifting hydrophone recorders. *J Acoust Soc Am* **144**(4):2030–2041. https://doi.org/10.1121/1.5055216

Chapman DMF (2008) Sinusoidal vertical motion of a sonobuoy suspension: experimental data and a theoretical model. *Ars J* **30**(2):179–185. https://doi.org/10.2514/8.5026

Ffowcs Williams JE, Hawkings DL (1969) Sound generation by turbulence and surfaces in arbitrary motion. *Philosophical Transactions of the Royal Society of London. Series A, Math Phys Sci* **264**(1151):321–342. https://doi.org/10.1098/rsta.1969.0031

Gobat JI, Grosenbaugh MA (1997) Modeling the mechanical and flow-induced noise on the surface suspended acoustic receiver. *1997 MTS/IEEE OCEANS*, Halifax, Canada, 748–754. https://doi.org/10.1109/OCEANS.1997.624086

Guan G, Geng J, Wang L (2020) Dynamic calculation for sonobuoy suspension heave reduction system with experimental correction. *Ocean Eng* 201:107141. https://doi.org/10.1016/j.oceaneng.2020.107141

Holler RA (2014) The evolution of the sonobuoy from World War II to the cold war. U.S. Navy J Underwater Acoustics **62**:322–347

Huang CL, Yang KD, Ma YL, Sun Q (2018) Flow noise calculation and suppression for sonobuoy. *2018 MTS/IEEE OCEANS*, Kobe, Japan, 1–4. https://doi.org/10.1109/OCEANSKOBE.2018.8559090

Huang CL, Yang KD, Li H, Zhang YK (2019) The flow noise calculation for an axisymmetric body in a complex underwater environment. *J Marine Sci Eng* **7**(9):1–17. https://doi.org/10.3390/jmse7090323

Kebe HW (1981) Self-noise measurements using a moored sonobuoy with a suspended hydrophone. *Mar Geophys Res* **5**(2):207–220. https://doi.org/10.1007/BF00163480

Kellett P, Turan O, Incecik A (2013) A study of numerical ship underwater noise prediction. *Ocean Eng* **66**(3):113–120. https://doi.org/10.1016/j.oceaneng.2013.04.006

Khalid MSU, Akhtar I, Wu B (2019) Quantification of flow noise produced by an oscillating hydrofoil. Ocean Eng **171**(1):377–390. https://doi.org/10.1016/j.oceaneng.2018.11.024

Kim KH, Yoon GH (2020) Aeroacoustic topology optimization of noise barrier based on Lighthill's acoustic analogy. *J Sound Vib* 483: 115512. https://doi.org/10.1016/j.jsv.2020.115512

Lauchle GC (1977) Noise generated by axisymmetric turbulent boundary-layer flow. *J Acoust Soc Am* **61**(3):694–703. https://doi.org/10.1121/1.381356

Li XG, Yang KD, Wang Y (2011) The power spectrum and correlation of flow noise for an axisymmetric body in water. *Chin Phys B* **20**(6): 269–276. https://doi.org/10.1088/1674-1056/20/6/064302

Lighthill MJ (1952) On sound generated aerodynamically: I. General theory. *Proc R Soc Lond A* **211**(1107):564–587. https://doi.org/10.2307/98943

Lighthill MJ (1954) On sound generated aerodynamically: II. Turbulence as a source of sound. *Proc R Soc Lond A* **222**(1148):1–32. https://doi.org/10.1098/rspa.1954.0049

McEachern JF (1995) Flow-induced noise on a bluff body. *J Acoust Soc Am* **97**(2):947–953. https://doi.org/10.1121/1.412073

Ozden MC, Gurkan AY, Ozden YA, Canyurt TG, Korkut E (2016) Underwater radiated noise prediction for a submarine propeller in different flow conditions. *Ocean Eng* 126:488–500. https://doi.org/10.1016/j.oceaneng.2016.06.012

Sea state table of wave and wind levels. Available at https://wenku.baidu.com/view/43059c6702768e9951e73818.html. [Accessed on Apr. 17, 2020]

Tahmasebi MK, Shamsoddini R, Abolpour B (2020) Performances of Different Turbulence Models for Simulating Shallow Water Sloshing in Rectangular Tank. *J Mar Sci Appl* **19**(3):381–387. https://doi.org/10.1016/0021-9991(92)90240-Y

Tan HP, Diamant R, Seah WKG, Waldmeyer M (2011) A survey of techniques and challenges in underwater localization. *Ocean Eng* **38**(14-15):1663–1676. https://doi.org/10.1016/j.oceaneng.2011.07.017

Tollefsen D, Sagen H (2013) Propagation of seismic exploration noise in the marginal ice zone. *J Acoust Soc Am* **133**(5):3398. https://doi.org/10.1121/1.4805910

Tollefsen D, Sagen H (2014) Seismic exploration noise reduction in the Marginal Ice Zone. *J Acoust Soc Am* **136**(1):EL47–EL52. https://doi.org/10.1121/1.4885547

Willis MR, Broudic M, Haywood C, Master I, Thomas S (2013) Measuring underwater background noise in high tidal flow environments. *Renewable Energy*, **49**(1): 255–258.10.1016/j.renene.2012.01.020

Yakhot V, Orszag SA, Thangam S, Gatski TB, Speziale CG (1992) Development of turbulence models for shear flows by a double expansion technique. *Phys Fluids A: Fluid Dynam* **4**(7):1510–1520. https://doi.org/10.1063/1.858424